A novel ion pseudo-trapping phenomenon within travelling wave ion guides

Sugyan M. Dixit,[†,‡] Keith Richardson,[ϰ,‡,*] David Langridge,[ϰ,‡] Kevin Giles,[ϰ] and Brandon T. Ruotolo[†,*]

[†] Department of Chemistry, University of Michigan, 930 North University Avenue, Ann Arbor, Michigan 48109, United States

[ϰ] Waters Corporation, Stamford Avenue, Altrincham Road, Wilmslow SK9 4AX, UK

ABSTRACT: The widespread use of traveling wave ion mobility (TWIM) technology in fields such as omics and structural biology motivates efforts to deepen our understanding of ion transport within such devices. Here, we describe a new advancement in TWIM theory, where pseudo-trapping within TW ion guides is characterized in detail. During pseudo-trapping, ions with different mobilities can travel with the same mean velocity, leaving others within the same TWIM experiment to separate as normal. Furthermore, pseudo-trapping limits typical band broadening experienced by ions during TWIM, manifesting as peaks with apparently improved IM resolving power, but all ions that undergo pseudo trapping are unable to separate by IM. SIMION simulations show that ions become locked into a repeated pattern of motion with respect to the TW reference frame during pseudo-trapping. We developed a simplified model capable of reproducing TW pseudo-trapping and reproducing trends observed in experimental data. Our model and simulations suggest that pseudo-trapping occurs only during experiments performed under static TWIM conditions, to an extent that depends on the detailed shape of the travelling wave. We show that pseudo-trapping alters the ion transit times and can adversely affect calibrated CCS measurements. Finally, we provide recommendations for avoiding unintentional pseudo-trapping in TWIM in order to obtain optimal separations and CCS determinations.

Ion mobility (IM) separation has been used for the physical and structural characterization of molecules for nearly 50 years[1–5]. The utility of IM is maximized when coupled to mass spectrometry (MS), as both ion size and m/z can be recorded rapidly in a manner that has proven to be enabling for areas ranging from food analyses to tissue imaging.[6–8] In recent years, IM-MS has gained traction as an approach for the system-wide analyses of cellular constituents[9–12] and in structural biology[13–15] due to its ability to obtain orientationally averaged collision cross-section (CCS) values used as restraints for bimolecular modeling[16–18]. Moreover, the development of commercial instruments, including those that incorporate drift tube IM (DTIM)[19], differential mobility spectrometry[20], traveling wave IM (TWIM)[21], trapped IM spectrometry (TIMS)[22], and structures for lossless ion manipulation (SLIM) devices[23], has spurred the widespread use of IM-MS over the past decade.[24] The introduction of TWIM technology[25] coupled to MS in a quadrupole/TWIM/oa-TOF platform [26] acted to significantly expand the user base of IM-MS technology[27]. A TWIM device is comprised of a radio frequency (RF) confined ion guide in which repeating DC pulses are applied sequentially to the electrodes in the device to create a traveling wave electric field (E). The wavelength λ is the distance between successive voltage maxima, and the traveling wave advances in steps of length d_s. In second generation TWIM instrumentation, $\lambda = 12$mm (eight electrodes) and $d_s = 3$ mm (two electrodes).

Higher mobility ion species are overtaken by the waves, resulting in a "roll-over" event, less often than low mobility species. The latter ions thus travel more slowly through a TWIM separator than the former, enabling a mobility-based separation[21,25,26,28,29]. However, due to the dynamic field and complex ion motion involved, obtaining an ion mobility value directly from observed TWIM arrival time distributions (ATDs) remains challenging. This necessitates the calibration of TWIM drift times using reference CCS values obtained from DTIM. Several studies have described the development of TWIM CCS calibration strategies using data acquired for various standards including small drug-like molecules[30], sugars[31], lipids[32], polynucleotides[33], peptides[34], proteins, and protein complexes[35]. Although several pioneering studies have developed theoretical frameworks that have enabled deeper insights into understanding the ion motion in TWIM[29,36–38], there are still deficiencies that make it challenging to predict characteristics of TWIM ATDs as well as obtain CCSs directly from TWIM measurements.

Here we observe and theoretically describe a novel pseudo-trapping effect within TW ion guides with implications for both TWIM separations and CCS determinations. Originally, the effect of pseudo-trapping was observed experimentally as a sharp increase in IM resolving power, defined as $t/\Delta t$, where t and Δt are the centroid and fwhm of TWIM ATDs, respectively. An ion trajectory simulation was used to investigate the origin of the effect, and it quickly became apparent that pseudo-trapping occurs when the roll-over period is close to an integer number of wave steps. Further numerical analysis showed that ions undergoing pseudo-trapping show a specific and repetitive pattern of motion causing species with different mobilities to travel with the same mean velocity. We present a theoretical framework to predict and describe such pseudo-trapping in TWIM. Theory and simulations suggest that TW waveforms that are not perfectly sinusoidal and smoothly

moving can exhibit the pseudo-trapping behavior we describe. We conclude by describing the impact of pseudo-trapping on the CCS calibration of TWIM measurements.

Experimental Section

Samples: Ubiquitin (U6253), cytochrome c (C2506), β-lactoglobulin (L7880), and D, L polyalanine (P9003) were purchased from Sigma-Aldrich, USA. Protein samples were prepared in 200 mM ammonium acetate solution at a concentration of 5 μM. Polyalanine was dissolved in 49.5%/49.5%/1% water/acetonitrile/acetic acid solution at 1 mg/ml final concentration.

TWIM-MS: All data was collected using a Synapt G2 instrument platform (Waters, Millford MA) [21,39]. Briefly, ions were generated using nano electrospray ionization (nESI) and then pulsed into the TWIM cell. TWIM device was operated at a pressure of 3.5 mbar with a combination of both He and N_2 gas present. TWIM-MS data was acquired at values of wave amplitude (V) ranging from 20 to 40 V and values of wave velocity (v) ranging from 200 to 1000 m/s. After ions transit the TWIM cell, they are transferred to an orthogonal acceleration (oa) time of flight (ToF) mass analyzer through a TW ion guide. TWIM ATDs are recorded through synchronization of oa-ToF acquisition with the gated release of ions from the trap into the TWIM cell. CCS was calibrated at all values of V and v using methods previously described[40].

SIMION Simulations: SIMION 8.1[41] was used to model ion transport within the TWIM cell[25]. By fixing ion motion to the axial direction, and removing RF confinement and velocity relaxation, a simplified 1 dimensional (1D) model was employed to study ion motion traces and investigate the effects of anharmonicity and wave stepping. A full off-axis 3 dimensional model (3D) with RF confinement, SDS gas model for diffusion, and velocity relaxation was also used. About ~1000 or more trajectories were created to accumulate a sufficient distribution of drift time values for analysis.

Data Analysis: TWIM ATD data was extracted using TWIMExtract[42]. ATDs were fitted with a Gaussian function to obtain t and Δt. CCS was calibrated using a power-law function as described previously[40]. Data were analyzed using python, numpy, and scipy[43,44] with in-house written scripts. Scipy.signal.find_peaks was used to obtain the γ values at pseudo-trapping regimes seen in Figures 1 and 2. Matplotlib[45] was used to generate all the plots.

Theory: a predictive model for pseudo-trapping in TWIM

In this section, we derive a predictive model for pseudo-trapping in TWIM. Detailed descriptions of the TWIM device can be found elsewhere.[21,25,26] For an ideal one-dimensional smoothly traveling sinusoidal wave with wavelength $\boldsymbol{\lambda}$, the roll-over period T is given exactly by:

$$T = \frac{\lambda}{v}\frac{1}{\sqrt{1-\gamma^2}} \#(1)$$

where $k = 2\pi/\lambda$, v is the wave velocity,

$$\gamma = \frac{kKV_0}{v} \#(2)$$

k is the wave number, K is ion mobility, and V_0 is the amplitude of the wave potential.[29] The parameter γ can be thought of as an effective wave height rescaled such that, for an ion of mobility K, the value $\gamma = 1$ corresponds to the onset of "surfing" in which the ions are simply pushed along at the speed of the wave. Useful separations are possible only for $\gamma < 1$.

As described above, pseudo-trapping appears to occur at values of γ for which the roll-over period T is close to an integer multiple m of the wave step period:

$$T = m\, t_s \#(3)$$

where the wave step period:

$$t_s = \frac{d_s}{v} \#(4)$$

and d_s is the wave step distance. For the second generation Synapt TWIM instrument (used in this study), wave step distance is equivalent to the width of a single pair of electrodes, i.e. 3 mm.[21]

We can use our idealized analytical model to find values of γ where this will happen. Rearranging Eq. 3 and substituting T and t_s from Eqs. 1 and 4, respectively, we arrive at:

$$m = \frac{T}{t_s} = \frac{\lambda}{d_s}\frac{1}{\sqrt{1-\gamma^2}} = \frac{n}{\sqrt{1-\gamma^2}} \#(5)$$

where:

$$n = \frac{\lambda}{d_s} \#(6)$$

is the number of wave steps in a wavelength. By re-arranging equation 5 we predict pseudo-trapping in TW ion guides at values of γ close to:

$$\gamma = \sqrt{1-\frac{n^2}{m^2}} \# (7)$$

for all integers $m > n$. For second generation TWIM instruments, $n = 4$. The limiting case $m = n$ occurs when the period of the wave is the same as the rollover period T so that $\gamma = 0$ and the ion is stationary.

Theory: a model system describing pseudo-trapping in TWIM

The motion of ions in real travelling wave devices is complicated, involving 3D RF effects, diffusion, velocity relaxation and wave stepping. It is therefore informative to try to find a minimal model dynamical system that exhibits pseudo-trapping. In the absence of velocity relaxation, ion motion in an idealized 1D TWIM device utilizing a smoothly moving sinusoidal waveform can be described, in the reference frame of the travelling wave, using[26]:

$$\frac{dz}{dt} = \gamma\, sin\, z - 1 \#(8)$$

where:

$$z = kx - \omega t + \varphi \#(9)$$

$\omega = 2\pi\, v/\lambda$ is the angular frequency, and φ is a phase constant. In this reference frame, wave steps appear as a time dependent phase shift as:

$$\frac{dz}{dt} = \gamma\, sin\big(z + \delta(t)\big) - 1 \;\#(10)$$

where $\delta(t)$, a sawtooth function, can be expanded as a Fourier series:

$$\delta(t) = \frac{\pi}{4} - \frac{1}{2}\sum_{n=1}^{\infty}\frac{1}{n} sin\; 4nt \;\;\#(11)$$

By taking only the first term from the expansion in Eq. 11, we obtain a wave that oscillates back and forth in the TW frame:

$$\delta(t) = -\zeta\; cos\; \Omega t \;\#(12)$$

where ζ is the amplitude of oscillation in z, and Ω is the angular frequency. Finally. by adding anharmonicity to Eq. 8 our model system becomes capable of reproducing pseudo-trapping in the TW reference frame:

$$\frac{dz}{dt} = \gamma\left(sin\big(z + \delta(t)\big) + asin3\big(z + \delta(t)\big)\right) - 1 \;\#(13)$$

where a is a factor controlling the degree of anharmonicity, allowing us to investigate how the shape of the TW form gives rise to pseudo-trapping.

Results and Discussion

During our previous efforts to establish an empirical model for describing TWIM ATDs[46], we observed an aberrant trend in $t/\Delta t$ at certain TW amplitudes and velocities. Figure 1a, b, and c show $t/\Delta t$ as a function of γ for ubiquitin 5^+, cytochrome c 6^+, and β-lactoglobulin 8^+ ions, respectively. Values of γ are calculated from Eq. 2 using nominal pressure and temperature and reference CCS values to obtain K. The trend seen in Figure 1 agrees well with our previous model[46] except at γ values of ~0.67 and ~0.82 , where we observe a significant increase in $t/\Delta t$**.** Our data shows an increase of 63%, 100%, and 200% in apparent TWIM resolving power for ubiquitin 5^+, cytochrome c 6^+, and β-lactoglobulin 8^+ ions, respectively, at γ~0.67 (Figures 1, S1, and S2). Comparison of the arrival time distributions with or without the pseudo-trapping effect is shown in Figure S1. Enhancements in apparent TWIM resolving power are smaller at γ~0.82, with $t/\Delta t$ increases of less than 20% in all cases. This, to our knowledge, is the first observation of such abrupt changes in TWIM resolving power. The gradual onset of the pseudo-trapping phenomenon is likely a result of diffusion as discussed further below. In order to begin ascribing a mechanism to the observations shown in Figure 1, we first investigated the potential role of ion heating induced structural changes on TWIM resolving power at the γ values indicated above. We calculated the field strengths necessary to remain within "low-field" conditions for the ions investigated in this study using previously described formulae [29]. The large number of rotational and vibrational degrees of freedom found in the protein ions studied here make it highly unlikely for significant ion heating to occur under our experimental conditions. We therefore interpret the abrupt increases in $t/\Delta t$ observed in Figure 1 as evidence of pseudo-trapping within TW ion guides.

The numerical models and simulations described above are able to successfully reproduce the changes in $t/\Delta t$ displayed in Figure 1. Figure 2a shows γ values computed

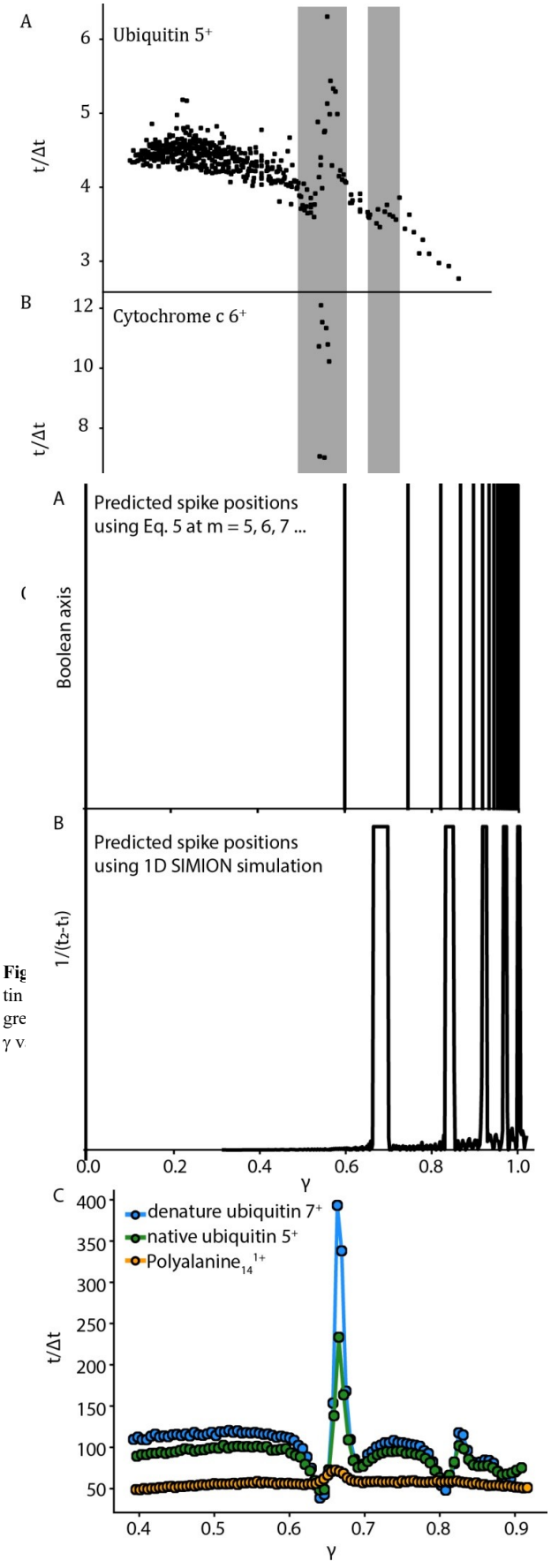

Figure 2. Prediction of increases in TWIM $t/\Delta t$ using both numerical models and simulations. A plot of increased $t/\Delta t$ positions in γ using Eq. 5. (A) and using 1D SIMION simulations (B) with a 3 mm wave step for denatured cytochrome c 19+ ions. C) A plot of $t/\Delta t$ as a function of γ using a 3D SIMION simulation for denatured ubiquitin, native ubiquitin, and poyalanine$_{14}^{1+}$ ions.

using Eq. 5 that are predicted to give rise to pseudo-trapping. Specifically, we predict that pseudo trapping should occur at γ values of 0.60, 0.74, and 0.82, corresponding to m = 5, 6, and 7, respectively. The quantitative discrepancy between the predicted and experimentally observed γ values (Figure 1) is likely a result of missing detail in the idealized model used to derive Eq. 7 such as the lack of wave stepping and anharmonicity. To perform similar predictions using our simplified 1D SIMION simulations with a 3 mm step wave, we created two ions of identical K 0.5 mm apart at the start of the simulation run and tracked the drift time over a range of TW voltages. Figure 2b plots the inverse of the drift time difference between these two test ions $1/(t_2 - t_1)$ over a range of γ values. At γ values similar to those discussed above in the context of Figure 2a, the difference in drift time between the two test ions becomes small, causing a large increase in $1/(t_2 - t_1)$. Predicted γ values for ion pseudo-trapping in Figure 2b match those observed experimentally (Figure 1). Finally, using a 3D velocity relaxed SIMION m odel, we obtained simulated distributions of ion arrival times for denatured ubiquitin 7^+, native ubiquitin 5^+, and polyalanine$_{14}^{1+}$ ions at a range of γ values to compare with our experimental observations. A plot of $t/\Delta t$ values obtained from these simulations as a function of γ is shown in Figure 2c. Here, we observe dramatic increases in $t/\Delta t$ at γ values that match the experimental observations in Figure 1. The relatively small effect observed for the polyalanine ion in Figure 2c deserves comment. The polyalanine ion is singly charged and much smaller than the ubiquitin ions, therefore while of comparable mobility it has a higher diffusion coefficient. It appears, therefore, that ions can escape the relatively weak pseudo trap by diffusion. Simulation of the polyalanine ion with the diffusion coefficient artificially halved shows a feature more comparable to the ubiquitin ions, lending support to this interpretation.

In order to investigate ion pseudo-trapping within TW ion guides in additional detail, we utilized our 1D SIMION model to produce ion trajectories for cytochrome c 19^+ ions at TW amplitudes ranging from 22 V to 27 V. Figure 3a shows the ion arrival time as a function of TW amplitude for these 1D simulations. As TW amplitude is increased, we observe a general decrease in ion transit time. However, we observe a plateau in ion residence time between TW amplitude values of 24.3 V to 25.6 V. Over this range of TW amplitudes ions are traveling at the same mean velocity in our simulations, and are thus pseudo-trapped within the guide. We examined simulated ion position data at TW amplitudes positioned either within or just outside of this plateau region (Figure 3b-e). For TW amplitudes outside the plateau we observe that the density of ion occupation is smoothly distributed with a greater concentration on the crest of the TW field than at other positions within the TW reference frame, suggesting that ions are experiencing roll-over events as is expected in normal TWIM separation (Figure 3b and 3c). However, during pseudo-trapping, we observe a sharp peak of ion occupation located at 3 mm with respect to (w.r.t.) the TW frame (Figure 3d and 3e). By examining the ion trace as a function of time (Figure 3d), we observe ions experiencing a repeating pattern of motion with a period of five wave steps. During one of the wave steps (i.e. 20% of the time) the ion occupies a specific position in the TW reference frame, which is not the case in the absence of pseudo-trapping (Figure 3b). These unusual features of ion motion observed in our simulations appear to explain our experimental observation (Figure 1), as the repeating pattern of ion motion we identify in Figure 3d leads our test ions to travel with the same mean velocity across a range of TW potentials and exhibit diminished diffusional broadening.

In order to understand the origin of pseudo-trapping in TWIM, we used our simulations and theoretical model to investigate the relationship of the shape of the TW field to the overall phenomenon. Figure 4a plots the average period T (using the model given by Eq. 13) as a function of γ employing various anharmonicity scaling factors (a). When a perfectly sinusoidal waveform is used, T increases smoothly with increasing γ. However, when anharmonicity is increased, a plateau in T develops over a range of γ values (Figure 4a). The range of γ values for which T remains con-

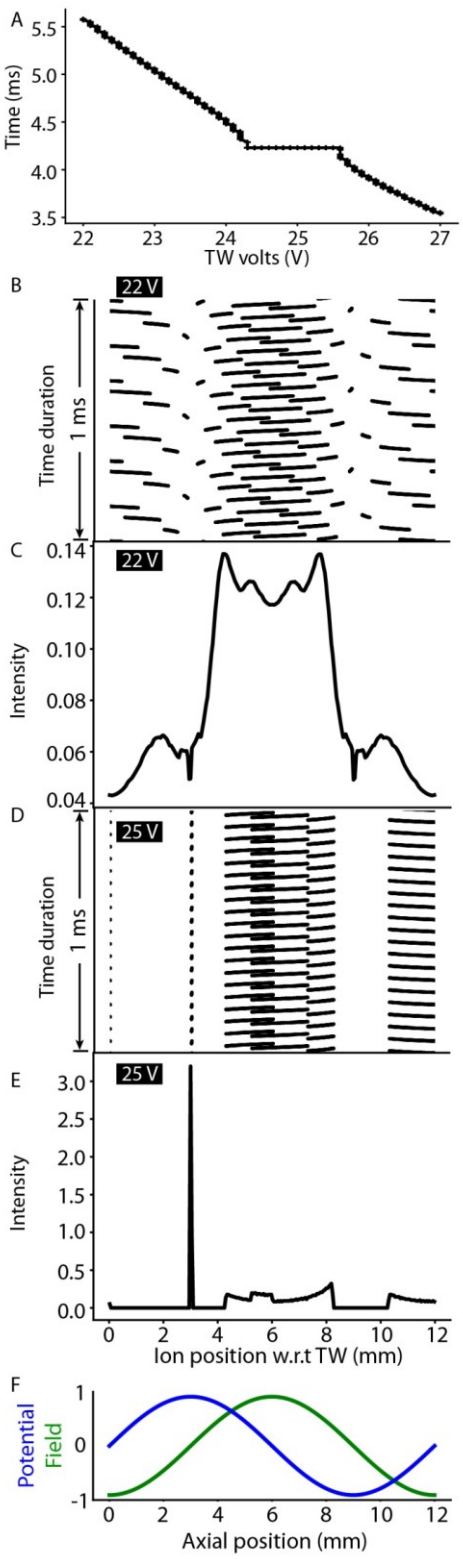

Figure 3. A) A plot of ion transit time as a function of TW volts. The plateau in the time domain indicates pseudo-trapping. B) and D) show traces of ion position w.r.t. the TW frame as a function of time at TW amplitudes of 22 V and 25 V, respectively. C) and E) are histogram plots showing ion occupancy as a function of ion position w.r.t. the TW frame at TW amplitudes of 22 V and 25 V, respectively. F) A plot of TW field and potential as a function of axial

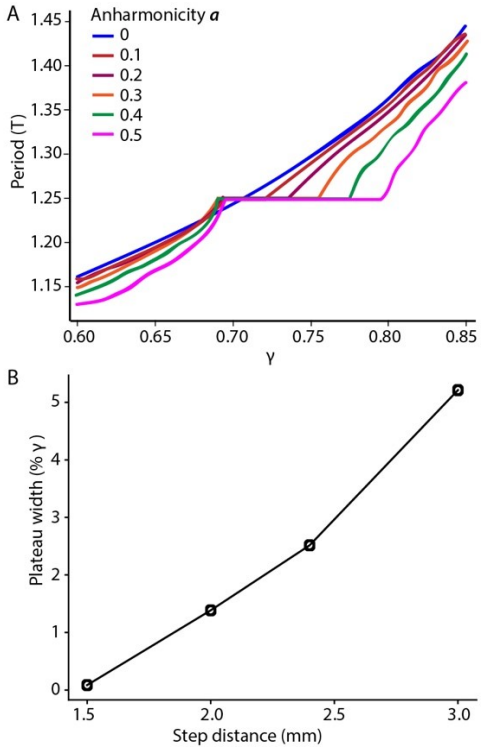

Figure 4. A) A plot of average period as a function of γ at various anharmonicity scaling factors (*a*) generated using Eq. 13. The width of the plateau in γ increases as a function of *a*. B) Plot showing plateau width in % γ as a function of wave step distance using a 1D SIMION simulation.

stant also increases with increasing anharmonicity. In our 1D SIMION simulation, we investigated the behavior of the plateau as a function of TW step distance (Figure 4b) and observed that the plateau width increases as a function of increasing step distance. Note that at a step distance of 1.5mm the plateau width is near zero, suggesting that a modification to our experimental system utilizing 1.5mm steps would not exhibit pseudo-trapping. Thus, both our theoretical model and simulations suggest that anharmonicity and wave stepping contribute to the pseudo-trapping phenomenon.

Finally, we investigated how pseudo-trapping of ions in TWIM affects calibrated CCS values. We determined experimental CCS values of cytochrome c 6^+ and β-lactoglobulin 8^+ ions using calibration over a broad range of γ values. Figure 5a shows the correlation coefficient R^2 from the CCS calibration as a function of γ. The R^2 values determined are in excess 0.99 at the majority of γ values, but R^2 decreases to 0.956 at a γ value of ~0.67, which is associated with pseudo-trapping (Figure 5a). This indicates that the fitness of TWIM CCS calibration is adversely affected when calibrant ions undergo pseudo-trapping. Figure 5b plots the error in predicted CCS values for cytochrome c 6^+ and β-lactoglobulin 8^+ ions as a function of γ values. The experimental CCS values are within 1.5% of reference values for cytochrome c 6^+ and β-lactoglobulin 8^+ ions under all conditions not associated with pseudo-trapping (Figure 5b). However, during pseudo-trapping, the magnitude of CCS deviation increases up to 3% and 5% for cytochrome c 6^+ and β-lactoglobulin 8^+ ions, respectively (Figure 5b). We also performed CCS calibrations using ion transit times extracted from our 3D SIMION model. The trends in CCS deviation from these simulated data matches well with that observed for the experimental data as shown

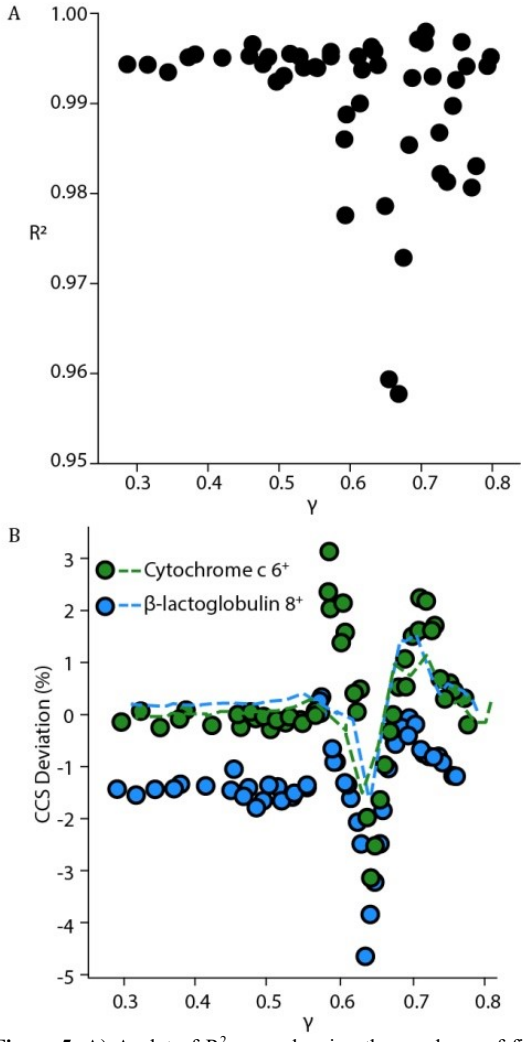

Figure 5. A) A plot of R^2 vs. γ showing the goodness of fit for CCS calibrations across a range of TW conditions. R^2 decreases dramatically during pseudo-trapping in TWIM. B) A plot of deviation (%) in CCS for predicted values from calibration vs. **γ** for cytochrome c 6^+ (green) and β-lactoglobulin 8^+ (blue) species where dots are experimental data and dashed lines are simulated data. The magnitude of CCS deviation increases during pseudo-trapping.

in Figure 5b. This indicates that pseudo-trapping can significantly alter ion transit times in TWIM leading to CCS calibrations of reduced accuracy.

Overall, this work suggests that TW pseudo-trapping of ions should be avoided in order to obtain reliable and accurate ATDs from TWIM analyzers. Under fixed TW amplitude and velocity conditions pseudo-trapping is avoided for $\gamma < 0.6$. For our experimental system, from rearrangement of Eq. 2, this corresponds to ensuring that $v/V_{TW} > 370\ K$, where V_{TW} is the TW pulse amplitude. Pseudo-trapping is also eliminated when TWIM is operated under ramped TW amplitude or velocity conditions.

Conclusions

In this study, we present a new development in TWIM theory that identifies conditions where pseudo-trapping occurs within TW ion guides. We observe a compression of TWIM ATD widths causing a spike in $t/\Delta t$ values under field conditions

predicted to lead to pseudo-trapping. Our numerical models and simulations can reproduce experimental results where we observe dramatic increases in apparent TWIM resolving power. By analyzing ion traces from simulations, we observe that ions follow a repetitive pattern of motion during pseudo-trapping, spending one out of every five wave steps at a position of 3 mm w.r.t. the TW frame during pseudo-trapping. This leads to ions having slightly different mobilities, or those experiencing slightly different TW potentials, to travel with the same mean velocity. We find that non-ideal waveforms, i.e. not perfectly sinusoidal and smoothly moving, exhibit pseudo-trapping at high values of γ. During pseudo-trapping, the centroid transit time, as well as the width of ion ATDs, are altered, leading to a reduction in the accuracy of calibrated CCS values from TWIM analyzers. Thus, in order to use TWIM devices to accurately obtain CCS values, pseudo-trapping conditions must be avoided. In future TW ion guide designs featuring either smoothly moving or near perfect sinusoidal waveforms should eliminate pseudo-trapping. We hope that further theoretical analysis of the phenomenon might reveal a connection to similar non-linear phenomena in other fields (e.g. Landau damping[48]).

By combining this work with our previous efforts to model TWIM ATDs, we are now approaching a nearly complete understanding of TWIM peak widths. In the future, we envision developing workflows for improved CCS calibration as well as the direct measurement of K from TWIM platforms. Such capabilities would leverage a growing population of TWIM analyzers[23,47] to perform ever more accurate assessments of ion CCS for applications in complex mixture analysis and structural biology. Furthermore, it is possible that future applications of TWIM, including those enabled by SLIM technologies, may benefit from the pseudo-trapping identified in this report, which enables a hybrid form of ion transport within TW ion guides.

ASSOCIATED CONTENT

AUTHOR INFORMATION

Corresponding Author

*_Brandon T. Ruotolo_ Phone: 1-734-615-0198. Fax: 1-734-615-3718. Email: bruotolo@umich.edu

*_Keith Richardson_ Email: keith_richardson@waters.com.

Author Contributions

‡These authors contributed equally**.** All authors have given approval to the final version of the manuscript.

ACKNOWLEDGMENT

B.T.R. and S.M.D. would like to acknowledge funding from the National Science Foundation Division of Chemistry under Grants 1808541 and 1253384 (with co-funding from the Division of Molecular and Cellular Biosciences) for supporting our efforts in TWIM theory development.

REFERENCES

(1) St Louis, R. H.; Hill Jr, H. H.; Alan Eiceman, G.; Hill, H. H.; Referee, J. Ion Mobility Spectrometry in Analytical Chemistry. *Crit. Rev. Anal. Chem.* **1990**, *21* (5), 321–355. https://doi.org/10.1080/10408349008050848org/10.1080/10408349008050848.

(2) Ewing, R. G.; Atkinson, D. A.; Eiceman, G. A.; Ewing, G. J. A Critical Review of Ion Mobility Spectrometry for the Detection of Explosives and Explosive Related Compounds. *Talanta* **2001**, *54* (3), 515–529. https://doi.org/10.1016/S0039-9140(00)00565-8.

(3) Puton, J.; Namieśnik, J. Ion Mobility Spectrometry: Current Status and Application for Chemical Warfare Agents Detection. *TrAC Trends Anal. Chem.* **2016**, *85*, 10–20. https://doi.org/10.1016/J.TRAC.2016.06.002.

(4) Hernández-Mesa, M.; Escourrou, A.; Monteau, F.; Le Bizec, B.; Dervilly-Pinel, G. Current Applications and Perspectives of Ion Mobility Spectrometry to Answer Chemical Food Safety Issues. *TrAC Trends Anal. Chem.* **2017**, *94*, 39–53. https://doi.org/10.1016/J.TRAC.2017.07.006.

(5) May, J. C.; Goodwin, C. R.; Lareau, N. M.; Leaptrot, K. L.; Morris, C. B.; Kurulugama, R. T.; Mordehai, A.; Klein, C.; Barry, W.; Darland, E.; et al. Conformational Ordering of Biomolecules in the Gas Phase: Nitrogen Collision Cross Sections Measured on a Prototype High Resolution Drift Tube Ion Mobility-Mass Spectrometer. *Anal. Chem.* **2014**, *86* (4), 2107–2116. https://doi.org/10.1021/ac4038448.

(6) Dodds, J. N.; Baker, E. S. Ion Mobility Spectrometry: Fundamental Concepts, Instrumentation, Applications, and the Road Ahead. *J. Am. Soc. Mass Spectrom.* **2019**, 1–11. https://doi.org/10.1007/s13361-019-02288-2.

(7) Beata M. Kolakowski, †; Paul A. D'Agostino, ‡; Claude Chenier, ‡ and; Zoltán Mester*, †. Analysis of Chemical Warfare Agents in Food Products by Atmospheric Pressure Ionization-High Field Asymmetric Waveform Ion Mobility Spectrometry-Mass Spectrometry. **2007**. https://doi.org/10.1021/AC070816J.

(8) McLean, J. A.; Ridenour, W. B.; Caprioli, R. M. Profiling and Imaging of Tissues by Imaging Ion Mobility-Mass Spectrometry. *J. Mass Spectrom.* **2007**, *42* (8), 1099–1105. https://doi.org/10.1002/jms.1254.

(9) McLean, J. A.; Ruotolo, B. T.; Gillig, K. J.; Russell, D. H. Ion Mobility–Mass Spectrometry: A New Paradigm for Proteomics. *Int. J. Mass Spectrom.* **2005**, *240* (3), 301–315. https://doi.org/10.1016/J.IJMS.2004.10.003.

(10) Helm, D.; Vissers, J. P. C.; Hughes, C. J.; Hahne, H.; Ruprecht, B.; Pachl, F.; Grzyb, A.; Richardson, K.; Wildgoose, J.; Maier, S. K.; et al. Ion Mobility Tandem Mass Spectrometry Enhances Performance of Bottom-up Proteomics □ S. *Mol. Cell. Proteomics* **2014**, *13*, 3709–3715. https://doi.org/10.1074/mcp.M114.041038.

(11) Zhang, X.; Quinn, K.; Cruickshank-Quinn, C.; Reisdorph, R.; Reisdorph, N. The Application of Ion Mobility Mass Spectrometry to Metabolomics. *Curr. Opin. Chem. Biol.* **2018**, *42*, 60–66. https://doi.org/10.1016/j.cbpa.2017.11.001.

(12) Paglia, G.; Astarita, G. Metabolomics and Lipidomics Using Traveling-Wave Ion Mobility Mass Spectrometry. *Nat. Protoc.* **2017**, *12*. https://doi.org/10.1038/nprot.2017.013.

(13) El-baba, T. J.; Woodall, D. W.; Raab, S. A.; Fuller, D. R.; Laganowsky, A.; Russell, D. H.; Clemmer, D. E. Melting Proteins: Evidence for Multiple Stable Structures upon Thermal Denaturation of Native Ubiquitin from IMS-MS Measurements. *J. Am. Chem. Soc.* **2017**, jacs.7b02774. https://doi.org/10.1021/jacs.7b02774.

(14) Allen, S. J.; Giles, K.; Gilbert, T.; Bush, M. F. Ion Mobility Mass Spectrometry of Peptide, Protein, and Protein Complex Ions Using a Radio-Frequency Confining Drift Cell. *Analyst* **2016**, *141* (3), 884–891. https://doi.org/10.1039/c5an02107c.

(15) Lanucara, F.; Holman, S. W.; Gray, C. J.; Eyers, C. E. The Power of Ion Mobility-Mass Spectrometry for Structural Characterization and the Study of Conformational Dynamics. *Nat. Chem.* **2014**, *6* (4), 281–294. https://doi.org/10.1038/nchem.1889.

(16) Politis, A.; Park, A. Y.; Hyung, S.-J.; Barsky, D.; Ruotolo, B. T. Integrating Ion Mobility Mass Spectrometry with Molecular Modelling to Determine the Architecture of Multiprotein Complexes. *PLoS One* **2010**, *5* (8), 12080. https://doi.org/10.1371/journal.pone.0012080.

(17) Eschweiler, J. D.; Frank, A. T.; Ruotolo, B. T. Coming to Grips with Ambiguity: Ion Mobility-Mass Spectrometry for Protein Quaternary Structure Assignment. *J Am Soc Mass Spectrom* **2017**. https://doi.org/10.1007/s13361-017-1757-1.

(18) Eschweiler, J. D.; Farrugia, M. A.; Dixit, S. M.; Hausinger, R. P.; Ruotolo, B. T. A Structural Model of the Urease Activation Complex Derived from Ion Mobility-Mass Spectrometry and Integrative Modeling. *Structure* **2018**, *26* (4), 599-606.e3. https://doi.org/10.1016/J.STR.2018.03.001.

(19) Ibrahim, Y. M.; Baker, E. S.; Danielson, W. F.; Norheim, R. V.; Prior, D. C.; Anderson, G. A.; Belov, M. E.; Smith, R. D. Development of a New Ion Mobility Time-of-Flight Mass Spectrometer. *Int. J. Mass Spectrom.* **2015**, *377*, 655–662. https://doi.org/10.1016/J.IJMS.2014.07.034.

(20) Kolakowski, B. M.; Mester, Z. Review of Applications of High-Field Asymmetric Waveform Ion Mobility Spectrometry (FAIMS) and Differential Mobility Spectrometry (DMS). *Analyst* **2007**, *132* (9), 842. https://doi.org/10.1039/b706039d.

(21) Giles, K.; Williams, J. P.; Campuzano, I. Enhancements in Travelling Wave Ion Mobility Resolution. *Rapid Commun. Mass Spectrom.* **2011**, *25* (11), 1559–1566. https://doi.org/10.1002/rcm.5013.

(22) Michelmann, K.; Silveira, J. A.; Ridgeway, M. E.; Park, M. A. Fundamentals of Trapped Ion Mobility Spectrometry. *J. Am. Soc. Mass Spectrom.* **2015**, *26* (1), 14–24. https://doi.org/10.1007/s13361-014-0999-4.

(23) Deng, L.; Webb, I. K.; Garimella, S. V. B.; Hamid, A. M.; Zheng, X.; Norheim, R. V.; Prost, S. A.; Anderson, G. A.; Sandoval, J. A.; Baker, E. S.; et al. Serpentine Ultralong Path with Extended Routing (SUPER) High Resolution Traveling Wave Ion Mobility-MS Using Structures for Lossless Ion Manipulations. *Anal. Chem.* **2017**, *89* (8), 4628–4634. https://doi.org/10.1021/acs.analchem.7b00185.

(24) May, J. C.; McLean, J. A. Ion Mobility-Mass Spectrometry: Time-Dispersive Instrumentation. *Anal. Chem.* **2015**, *87* (3), 1422–1436. https://doi.org/10.1021/ac504720m.

(25) Giles, K.; Pringle, S. D.; Worthington, K. R.; Little, D.; Wildgoose, J. L.; Bateman, R. H. Applications of a Travelling Wave-Based Radio-Frequency-Only Stacked Ring Ion Guide. *Rapid Commun. Mass Spectrom.* **2004**, *18* (20), 2401–2414. https://doi.org/10.1002/rcm.1641.

(26) Pringle, S. D.; Giles, K.; Wildgoose, J. L.; Williams, J. P.; Slade, S. E.; Thalassinos, K.; Bateman, R. H.; Bowers, M. T.; Scrivens, J. H. An Investigation of the Mobility Separation of Some Peptide and Protein Ions Using a New Hybrid Quadrupole/Travelling Wave IMS/Oa-ToF Instrument. *Int. J. Mass Spectrom.* **2007**, *261* (1), 1–12. https://doi.org/10.1016/j.ijms.2006.07.021.

(27) May, J. C.; Morris, C. B.; McLean, J. A. Ion Mobility Collision Cross Section Compendium. *Anal Chem* **2017**, *89* (2), 1032–1044. https://doi.org/10.1021/acs.analchem.6b04905.

(28) Shvartsburg, A. A.; Smith, R. D. Fundamentals of Traveling Wave Ion Mobility Spectrometry. *Anal Chem* **2008**, *80* (24), 9689–9699. https://doi.org/10.1021/ac8016295.

(29) Richardson, K.; Langridge, D.; Giles, K. Fundamentals of Travelling Wave Ion Mobility Revisited: I. Smoothly Moving Waves. *Int. J. Mass Spectrom.* **2018**, *428*, 71–80. https://doi.org/10.1016/J.IJMS.2018.03.007.

(30) Campuzano, I.; Bush, M. F.; Robinson, C. V.; Beaumont, C.; Richardson, K.; Kim, H.; Kim, H. I. Structural Characterization of Drug-like Compounds by Ion Mobility Mass Spectrometry: Comparison of Theoretical and Experimentally Derived Nitrogen Collision Cross Sections. *Anal. Chem.* **2012**, *84* (2), 1026–1033. https://doi.org/10.1021/ac202625t.

(31) Hofmann, J.; Struwe, W. B.; Scarff, C. A.; Scrivens, J. H.; Harvey, D. J.; Pagel, K. Estimating Collision Cross Sections of Negatively Charged *N*- Glycans Using Traveling Wave Ion Mobility-Mass Spectrometry. *Anal. Chem.* **2014**, *86* (21), 10789–10795. https://doi.org/10.1021/ac5028353.

(32) Hines, K. M.; May, J. C.; Mclean, J. A.; Xu, L. Evaluation of Collision Cross Section Calibrants for Structural Analysis of Lipids by Traveling Wave Ion Mobility-Mass Spectrometry. **2016**. https://doi.org/10.1021/acs.analchem.6b01728.

(33) Lippens, J. L.; Ranganathan, S. V; D'esposito, R. J.; Fabris, D. Modular Calibrant Sets for the Structural Analysis of Nucleic Acids by Ion Mobility Spectrometry Mass Spectrometry †. *Analyst* **2016**, *141*, 4084. https://doi.org/10.1039/c6an00453a.

(34) Bush, M. F.; Campuzano, I. D. G.; Robinson, C. V. Ion Mobility Mass Spectrometry of Peptide Ions: Effects of Drift Gas and Calibration Strategies. *Anal. Chem.* **2012**, *84* (16), 7124–7130. https://doi.org/10.1021/ac3014498.

(35) Bush, M. F.; Hall, Z.; Giles, K.; Hoyes, J.; Robinson, C. V.; Ruotolo, B. T. Collision Cross Sections of Proteins and Their Complexes: A Calibration Framework and Database for Gas-Phase Structural Biology. *Anal. Chem.* **2010**, *82* (22), 9557–9565. https://doi.org/10.1021/ac1022953.

(36) Shvartsburg, A. A.; Smith, R. D. Fundamentals of Traveling Wave Ion Mobility Spectrometry. *Anal. Chem.* **2008**, *80* (24), 9689–9699. https://doi.org/10.1021/ac8016295.

(37) Mortensen, D. N.; Susa, A. C.; Williams, E. R. Collisional Cross-Sections with T-Wave Ion Mobility Spectrometry without Experimental Calibration. *J Am Soc Mass Spectrom* **2017**, *28* (7), 1282–1292. https://doi.org/10.1007/s13361-017-1669-0.

(38) Kune, C.; Far, J.; De Pauw, E. Accurate Drift Time Determination by Traveling Wave Ion Mobility Spectrometry: The Concept of the Diffusion Calibration. *Anal Chem* **2016**, *88* (23), 11639–11646. https://doi.org/10.1021/acs.analchem.6b03215.

(39) Ruotolo, B. T.; Benesch, J. L.; Sandercock, A. M.; Hyung, S. J.; Robinson, C. V. Ion Mobility-Mass Spectrometry Analysis of Large Protein Complexes. *Nat Protoc* **2008**, *3* (7), 1139–1152. https://doi.org/10.1038/nprot.2008.78.

(40) Ruotolo, B. T.; Benesch, J. L. P.; Sandercock, A. M.; Hyung, S.-J.; Robinson, C. V. Ion Mobility–Mass Spectrometry Analysis of Large Protein Complexes. *Nat. Protoc.* **2008**, *3* (7), 1139–1152. https://doi.org/10.1038/nprot.2008.78.

(41) Manura, D.; Dahl, D. *SIMION (R) 8.0/8.1 User Manual*; Scientific Instrument Services: Ringoes, NJ, 2011.

(42) Haynes, S. E.; Polasky, D. A.; Dixit, S. M.; Majmudar, J. D.; Neeson, K.; Ruotolo, B. T.; Martin, B. R. Variable-Velocity Traveling-Wave Ion Mobility Separation Enhancing Peak Capacity for Data-Independent Acquisition Proteomics. *Anal. Chem.* **2017**, *89* (11), 5669–5672.

https://doi.org/10.1021/acs.analchem.7b00112.

(43) Oliphant, T. E. Python for Scientific Computing. *Comput. Sci. Eng.* **2007**, *9* (3), 10–20. https://doi.org/10.1109/MCSE.2007.58.

(44) Walt, S. van der; Colbert, S. C.; Varoquaux, G. The NumPy Array: A Structure for Efficient Numerical Computation. *Comput. Sci. Eng.* **2011**, *13* (2), 22–30. https://doi.org/10.1109/mcse.2011.37.

(45) Hunter, J. D. Matplotlib: A 2D Graphics Environment. *Comput. Sci. Eng.* **2007**, *9* (3), 99–104. https://doi.org/10.1109/MCSE.2007.55.

(46) Dixit, S. M.; Ruotolo, B. T. A Semi-Empirical Framework for Interpreting Traveling Wave Ion Mobility Arrival Time Distributions. *J. Am. Soc. Mass Spectrom.* **2019**, *30* (6), 956–966. https://doi.org/10.1007/s13361-019-02133-6.

(47) Giles, K.; Ujma, J.; Wildgoose, J.; Pringle, S.; Richardson, K.; Langridge, D.; Green, M. A Cyclic Ion Mobility-Mass Spectrometry System. *Anal. Chem.* **2019**, *91* (13), 8564–8573. https://doi.org/10.1021/acs.analchem.9b01838.

(48) Doveil, F; Escande, D. F.; Macor, A. Experimental Observation of Nonlinear Synchronization due to a Single Wave. *Phys. Rev. Lett*. **2005**, 94, 085003. https://doi.org/10.1103/PhysRevLett.94.085003

Table of Contents Graphic: